博士学位論文

Doctoral Dissertation

論文題目

Lipopolysaccharide-bound structure of the antimicrobial peptide cecropin P1 determined by nuclear magnetic resonance spectroscopy

(NMR 法による抗菌ペプチドセクロピン P1 の LPS 結合構造の解析)

白 美 花

BAEK Mihwa

北海道大学大学院生命科学院

Graduate School of Life Science, Hokkaido University

平成 28 年 6 月

Contents

Summary

Antimicrobial peptides (AMPs) are components of the innate immune system. AMPs may be potential alternatives to conventional antibiotics because they exhibit broad-spectrum antimicrobial activity activities against several organisms, such as Gram-negative and Gram-positive bacteria, viruses, and fungi.

The AMP cecropin P1 (CP1), isolated from nematodes found in the stomachs of pigs, is known to exhibit antimicrobial activity against Gram-negative bacteria with reduced activity against Gram-positive bacteria. In general, CP1 is believed to disrupt the inner membrane through the so-called 'carpet mechanism', allowing it to function while not entering the hydrocarbon core of the membrane. However, although CP1 is known to interact with the outer membrane of Gram-negative bacteria, the mechanisms and properties of these functions are not yet fully understood.

I investigated the interaction between CP1 and lipopolysaccharide (LPS) because LPS is the main component of the outer membrane of Gram-negative bacteria and AMPs first encounter and bind to negatively charged LPS. Therefore, elucidation of the detailed structures of AMPs bound to LPS will provide important information about the association between antimicrobial activity and the tertiary structure of the AMP.

In the present study, I examined the LPS-bound state of CP1 using circular dichroism (CD) spectroscopy and nuclear magnetic resonance (NMR) spectroscopy and evaluated its antimicrobial activity by minimum bactericidal concentration (MBC) measurements. CD results showed that CP1 formed an α-helical structure in a solution containing LPS. For NMR experiments, I expressed ^{15}N- and ^{13}C-labeled CP1 in bacterial cells and successfully assigned almost all backbone and side-chain proton resonance peaks of CP1 in water for transferred nuclear Overhauser effect (Tr-NOE)

experiments in LPS. I performed ^{15}N-edited and ^{13}C-edited Tr-NOE spectroscopy (Tr-NOESY) for CP1 bound to LPS. Tr-NOE peaks were observed at the only C-terminal region of CP1 in LPS. The results of structure calculation indicated that the C-terminal region (Lys15–Gly29) formed the well-defined α-helical structure in LPS. LPS-bound CP1 had a C-terminal α-helical structure including some positively charged residues (Lys15, Lys16, and Arg17) and hydrophobic residues (Ile18, Ile22, Ala23, Ile24, Ala25, and Ile26). The docking study revealed that CP1 was oriented parallel to the long axis of the lipid A portion of LPS. Especially, Lys15/Lys16 interacted with phosphate at GlcN I via an electrostatic interaction and that Ile22/Ile26 was in close proximity with the acyl chain of lipid A. One dimensional ^{31}P NMR measurement also showed the peak intensity of the ^{31}P resonance of LPS was significantly changed by binding to CP1. I determined the antimicrobial activity of CP1 and CP1 analogs lacking the C-terminal amino acid residues ($CP1_{1\text{-}25}$, and $CP1_{1\text{-}20}$) using *E. coli* ML35. The result indicated that the α-helical C-terminal region contributed to the antimicrobial activity of CP1 against Gram-negative bacteria.

The results of this study showed that the C-terminal α-helical structure of CP1 played a crucial role in the recognition of LPS. I anticipate that these findings will be useful for studies of LPS recognition by AMPs. This improved understanding of the molecular basis of AMP activity may assist in the future design of more specific and potent antibacterial agents.

Abstract

Antimicrobial peptides (AMPs) are components of the innate immune system and may be potential alternatives to conventional antibiotics because they exhibit broad-spectrum antimicrobial activity. The AMP cecropin P1 (CP1), isolated from nematodes found in the stomachs of pigs, is known to exhibit antimicrobial activity against Gram-negative bacteria. In this study, I investigated the interaction between CP1 and lipopolysaccharide (LPS), which is the main component of the outer membrane of Gram-negative bacteria, using circular dichroism (CD) and nuclear magnetic resonance (NMR). CD results showed that CP1 formed an α-helical structure in a solution containing LPS. For NMR experiments, I expressed ^{15}N- and ^{13}C-labeled CP1 in bacterial cells and successfully assigned almost all backbone and side-chain proton resonance peaks of CP1 in water for transferred nuclear Overhauser effect (Tr-NOE) experiments in LPS. I performed ^{15}N-edited and ^{13}C-edited Tr-NOE spectroscopy (Tr-NOESY) for CP1 bound to LPS. Tr-NOE peaks were observed at the only C-terminal region of CP1 in LPS. The results of structure calculation indicated that the C-terminal region (Lys15–Gly29) formed the well-defined α-helical structure in LPS. Finally, the docking study revealed that Lys15/Lys16 interacted with phosphate at GlcN I via an electrostatic interaction and that Ile22/Ile26 was in close proximity with the acyl chain of lipid A.

1. Introduction

The use of antibiotics has led to the emergence of multidrug-resistant bacteria, resulting in untreatable infections and nosocomial infections. Antimicrobial peptides (AMPs), components of the innate immune system, are being investigated as potential therapeutics to replace or complement traditional antibiotics. AMPs have broad spectrum antimicrobial activities against several organisms, such as Gram-negative and Gram-positive bacteria, viruses, and fungi [1]. Research groups have recently begun to focus on identification of natural AMPs, and over 1300 AMPs have been isolated from a variety of organisms. AMPs are classified based on their amino acid composition or structure as β-sheet, α-helical, loop, and extended peptides. Cecropins, histatins, defensins, and cathelicidins are well-known AMP families [2].

Cecropin P1 (CP1), a 31-amino acid cationic antimicrobial peptide isolated from nematodes found in the stomachs of pigs [3], has antimicrobial activity against a variety of Gram-negative bacteria, with reduced activity against Gram-positive bacteria [4]. CP1 has been reported to have antimicrobial activity against many clinically relevant Gram-negative bacteria, including *Pseudomonas aeruginosa* and *Acinetobacter baumannii* [5,6]. Additionally, CP1 has the potential to replace antibody-based biosensors owing to its ability to selectively bind to microbial cell surfaces, e.g., pathogenic *Escherichia coli* [7–9]. In general, CP1 is believed to disrupt the inner membrane through the so-called ‘carpet mechanism’, allowing it to function while not entering the hydrocarbon core of the membrane. The membrane disintegrates owing to disruption of lipid packing within the bilayer, i.e., interactions between negatively charged amino acids and the positively charged head groups of the phospholipids and the orientation of the hydrophobic residues toward the hydrophobic core of the

membrane [10]. However, although CP1 is known to interact with the outer membrane of Gram-negative bacteria, the mechanisms and properties of these functions are not yet fully understood [4].

Lipopolysaccharide (LPS) is the major constituent of the outer leaflet of the outer membrane in Gram-negative bacteria and functions as a permeability barrier against a variety of molecules [11]. Also known as endotoxin, LPS is released from bacteria during cell division, during cell death, or as a result of antibiotic treatment. The complex structure of LPS consists of three parts: an outer O-antigen segment, the core oligosaccharide, and the lipid A portion [12]. Many studies have been reported that AMPs first encounter and bind to negatively charged LPS [13–15]. Therefore, elucidation of the detailed structures of AMPs bound to LPS will provide important insights into the association between antimicrobial activity and the tertiary structure of the AMP. A structural study of CP1 in a hydrophobic environment [16] showed that CP1 exhibits a straight α-helical structure (Lys3-Gly29), which is different from other insect cecropin structures harboring the two helices connected by a hinge [17,18]. However, no studies have reported the LPS-bound structure of CP1.

In the present study, I examined the structure of CP1 in the presence of LPS using circular dichroism (CD) spectroscopy and nuclear magnetic resonance (NMR) spectroscopy and evaluated its antimicrobial activity by minimum bactericidal concentration (MBC) measurements. I attempted to obtain isotopically labeled recombinant peptide samples for NMR and then applied these samples to transferred nuclear Overhauser effect (Tr-NOE) experiments, which allow for structural analysis of high-molecular-weight complexes that cannot be studied by traditional NMR [19], to determine the high-resolution structure of CP1 bound to LPS. Based on NMR data, I

successfully identified the tertiary structure of CP1 in LPS. Subsequently, important residues involved in LPS binding were determined by molecular docking simulations.

2. Materials and Methods

2.1 Preparation of peptide samples

Chemically synthesized CP1 (SWLSKTAKKLENSAKKRISEGIAIAIQGGPR) and the truncated analogs $CP1_{1-25}$ and $CP1_{1-20}$ were prepared by Fmoc solid-phase chemistry (Sigma Life Science).

For preparation of stable isotopic labeled CP1, *Escherichia coli* BL21(DE3) was used as the expression host, and pET32a(+) was used as the expression plasmid. I designed a soluble fusion protein that contained thioredoxin (TRX) on the N-terminal side of CP1 to decrease the toxic effects of AMPs in the host cells and to protect small AMPs from proteolytic degradation [20]. Chemically synthesized DNA fragment encoding the mature region of CP1 was amplified using PCR. The synthetic oligonucleotides encoding CP1 with codon optimization for *E. coli* (AGCTGGCTGAGCAAAACCGCGAAAAAACTGGAAAACAGCGCGAAAAAAC GTATTAGCGAAGGCATTGCGATTGCGATTCAGGGCGGCCCGCGT) were used as a template, with appropriate primers (forward: ATGAGATCTGGACGACGACGACAAGAGCTGGCTGAGCAAAACCG, reverse: TTAACGCGGGCCGCC) for PCR. A *Bgl*II endonuclease site (underlined) and enterokinase cleavage site were included at the end of the forward primer, and the stop codon TAA was incorporated at the end of the reverse primer. The purified PCR products were digested with *Bgl*II, and the plasmid vector pET32a (+) was digested with *Bgl*II and *Eco*RV and then ligated. For uniform ^{15}N and ^{13}C enrichment of the peptides, cells were grown in minimal medium that included ^{13}C-labeled glucose and ^{15}N-labeled ammonium chloride. The fusion proteins were purified by Ni-nitrilotriacetic acid affinity chromatography, and the target peptide was obtained by enterokinase

cleavage of the fusion protein followed by reverse-phase high-performance liquid chromatography (RP-HPLC). A total of 3.5 mg CP1 was purified from 1 L of *E. coli* culture.

2.2 CD measurements

All CD data were acquired using a Jasco J-725 spectropolarimeter (Jasco) using a quartz cell with a 1-mm path length. The spectra were recorded between 190 and 250 nm with a data pitch of 0.2 nm, a bandwidth of 1 nm, a scanning speed of 50 nm/min, and 8 scans at 25°C. The CP1/LPS solution contained 20 μM CP1, 10 mM sodium phosphate (pH 6.0), and 0–100 μM LPS. The average of eight scans was determined for each sample after subtracting the average of the blank and LPS spectrum.

2.3 NMR measurement

All NMR spectra were recorded on a BRUKER DMX 600 MHz equipped with a cryo-probe at a temperature of 298 K. CP1 (unlabeled and ^{15}N, ^{13}C-labeled CP1) was dissolved at a concentration of 1 mM in 90% H_2O/10% D_2O at pH 5.0. ^{1}H NMR experiments were performed with 1 mM CP1 samples titrated with various concentrations of LPS (5–200 μM) to determine the appropriate conditions for NMR measurement. Two-dimensional (2D) ^{1}H-^{15}N heteronuclear single quantum correlation (HSQC), ^{15}N-edited Tr-NOESY, and ^{13}C-edited Tr-NOESY experiments were recorded at the CP1/LPS concentration of 1 mM/50 μM and at mixing times of 150 and 300 ms [19]. Data were processed using NMRPipe 4.1 and NMRDraw 2.3 and analyzed using Sparky 3.113 software [21,22].

2.4 Structural calculation

The NOE cross-peaks from the three-dimensional (3D) ^{15}N-edited NOESY and ^{13}C-edited NOESY spectra of CP1 were assigned using Sparky 3.113 software. A total of 387 NOEs were used for structural calculation, and the NOE-based distance restraints were derived based on the peak volume. For structural calculations, I used NOEs observed only in the LPS-bound state or clearly increased in their intensities from the free state to the LPS-bound state. The peptide structures were determined using the CYANA 2.1 program [23]. A total of 100 structures were examined using the PROCHECK-NMR program to identify the 20 structures with the lowest energy [24]. Structures were visualized using PyMOL 1.7 [25]. NMR resonance assignments for CP1 in LPS have been deposited in Biological Magnetic Resonance Bank (BMRB ID 25877). The structural coordinates of CP1 in LPS have been deposited in the Protein Data Bank (PDB ID 2n92).

2.5 Molecular docking of LPS-bound CP1

Using the CP1 structure calculated from the distance restraints of Tr-NOE, docking simulation of CP1 and LPS was performed with the AutoDock Vina program [26]. LPS was used as a receptor, and the 3D structure of LPS was obtained from the protein data bank (PDB ID 1QFG) [27]. Docking calculations were carried out based on the protocol described by Bhunia *et al.* [28]. The backbones of the peptide and LPS were set rigid whereas almost all side chains of CP1 were defined as flexible using Autodock tools (ADT). The docking was blind, with a grid box of 70 × 80 × 80 points, grid spacing of 0.375 Å, and the H2 atom of the glucosamine II (GlcN II) in lipid A set as the grid center. Docking calculations were carried out using a Lamarchian genetic

algorithm (LGA) with a translation step of 0.2 Å, a quaternion step of 5°, and a torsion step of 5°. The maximum number of energy evaluations increased to 15,000,000. Two hundred LGA docking runs were performed.

2.6 Antimicrobial activity

The antimicrobial activity of CP1 and its analogs, $CP1_{1-25}$ and $CP1_{1-20}$, were measured using *E. coli* ML35 (ATCC 43827). Overnight culture was added to fresh TSB broth and further cultured at 37°C with shaking at 180 rpm. *E. coli* cultures were harvested when the OD_{660} value was about 0.4 and centrifuged. The precipitate was washed in 10 mM sodium phosphate buffer (pH 7.4) supplemented 1% medium and was resuspended in the same buffer. Bacterial suspensions (1×10^8 CFU/mL) were incubated with the peptide in a total volume 50 μL for 5 min at 37°C with shaking at 180 rpm. Following incubation, samples were diluted, and 50-μL aliquots of samples were plated on TSB agar plates. Surviving bacterial rates were determined relative to the surviving colonies of untreated control cultures after 12–14 h of incubation at 30°C. The MBC was determined by the lowest concentration of peptide that ablated the bacterial colony growth on the agar plate.

3. Results

3.1 CD measurement of CP1 with LPS

CD spectroscopy is a useful tool for determining the secondary structures and binding properties of proteins [29]. Figure 1 shows the CD spectra of 20 μM CP1 with or without LPS in pH 6. I checked the pH dependence of the CD spectra and did not observe any significant structural changes (data not shown). I used various concentrations of LPS ranging from 5 to 100 μM to determine concentration-dependent changes in the peptide conformation. In the aqueous solution, CP1 showed a strong negative band at 200 nm, indicating that CP1 exhibited a random-coil conformation in water. As the concentration of LPS increased, the CD spectra revealed some helical tendencies, with a positive peak at 195 nm and two negative peaks at 208 and at 222 nm. In the presence of higher than 80 μM LPS, the binding transition was likely to be saturated. However, the spectrum in the presence of 100 μM LPS seemed less helical than that in the presence of 80 μM LPS. This result may suggest that the peptide exhibited an additional conformational change at higher concentrations of LPS. At a concentration of 80 μM LPS, CP1 possessed 75.57% α-helical content using K2D3 [30].

3.2 Tr-NOESY of CP1 in the LPS-bound state

I obtained the ^{1}H NMR spectra of 1 mM CP1 with various concentrations of LPS (10–200 μM) to identify the appropriate conditions for NMR experiments. The critical micelle concentration (CMC) value of LPS from *E. coli* O111:B4 has been estimated to be 1.3–1.6 μM, with an aggregation number of 43–49 molecules per micelle at a concentration of 2 μM LPS [31]. From these parameters, the micelle size was assumed to be about 500 kDa. Detailed NMR analysis was not easy because LPS

formed large micelles at a concentration of 50 μM, which resulted in line-shape broadening. The ^{1}H-NMR spectra of CP1 in the presence of LPS showed concentration-dependent moderate line-shape broadening and slight changes in chemical shift, indicating rapid exchange (data not shown). This result suggested that CP1 underwent a rapid exchange between free and LPS-bound states in the NMR time scale. Tr-NOESY spectra of CP1 with LPS under conditions in which the line-broadening of CP1 resonances was observed; this experiment is a useful tool to determine 3D structures of ligands bound to the macromolecules [19,32]. Figure 2 shows the ^{1}H-^{1}H 2D NOESY spectra of CP1 without (Figure 2A) or with (Figure 2B) LPS. Both NOE crosspeaks of free CP1 and CP1 with LPS exhibited negative NOE peaks, suggesting that both had a high molecular weight. In the presence of LPS, the 2D Tr-NOESY spectrum of CP1 showed a significant increase in the number of NOE cross-peaks. I found new NOE cross-peaks within the entire region, particularly in the HN-HN region. However, I could not assign many NOE cross-peaks exactly due to resonance overlap. Thus, I prepared isotope-labeled CP1 samples for efficient NMR experiments and NOE analysis to overcome the difficulties in signal assignment.

3.3 NMR resonance assignments

2D ^{1}H-^{15}N HSQC spectra of CP1 were obtained at 298 K and pH 5.0 (Figure 3). I successfully assigned almost all backbone and side-chain protons resonance peaks with triple resonance experiments, although there were some minor peaks caused by impurities in the sample. Sequence-specific resonance assignment was achieved by analyzing CBCACONH, HNCACB, CBCANH, HNCA, HNCACO, HNCO, ^{15}N-edited TOCSY, and HCCCONH spectra. The ^{15}N, ^{13}C, and ^{1}H chemical shift assignments of

CP1 are summarized in Supporting Information Table S1.

3.4 Structural analysis of CP1 with LPS

In order to determine the structure of CP1 bound to LPS, I applied 3D ^{15}N-edited Tr-NOESY and 3D ^{13}C-edited Tr-NOESY experiments [19,32]. I could assign almost all NOE cross-peaks in the 3D Tr-NOESY spectra. Similar to 2D NOESY spectra, representative NOE cross-peaks patterns between the HN-HN region and aliphatic hydrogen regions were observed in the spectrum of CP1 in presence of LPS. Figure 4 shows a summary of the sequential and medium-range NOEs used to determine the secondary structure of CP1 bound to LPS. Representative NOE correlations ($d_{NN}(i,i+1)$ NOEs and several medium-range NOEs, such as $d_{NN}(i,i+2)$, $d_{\alpha N}(i,i+3)$, and $d_{\alpha\beta}(i,i+3)$ correlations) indicated that LPS-bound CP1 exhibited an α-helical structure between residues Lys15 and Gly29. The calculated helical content was 48%. This result was in disagreement with the results of CD spectroscopy. However, previous studies have shown that, for some peptides, the CD and NMR results may be dissimilar [33]. In this previous study, in TFE or micelle solutions, a trend toward higher estimation of helical contents by CD was observed. Thus, the LPS micelle solution may have affected the results of CD spectroscopy in my current study. Many NOE connectivities were observed, indicating that the C-terminal region of CP1 formed a well-folded conformation. On the other hand, NOE correlations in the N-terminal region were not observed. This result indicated that the N-terminal region of CP1 did not form a well-defined structure.

The 3D structure of LPS-bound CP1 was determined from NOE-derived distance restraints using a total of 387 NOEs obtained from Tr-NOESY spectra. These

NOE peaks resulted in 337 meaningful distance constraints. The number of experimental restraints and NMR statistics are shown in Table 1. All the constraints were used to generate a total of 100 structures, among which the 20 with the lowest target function were selected and energy minimized. Figure 5 shows the backbone traces of the 20 lowest energy structures of LPS-bound CP1. As shown in Figure 5, CP1 exhibited an α-helical structure in the C-terminal region (Lys15 to Gly29). The backbone and heavy-atom RMSD for this structurally defined region of CP1 were low (about 0.15 and 0.68 Å, respectively). In contrast to the C-terminal region, the N-terminal region (Ser1–Ala14) did not form a well-defined structure.

The surface representation shown in Figure 6 describes the electrostatic surface potential of CP1 bound to LPS. LPS-bound CP1 had a C-terminal α-helical structure including some positively charged residues (Lys15, Lys16, and Arg17) and hydrophobic residues (Ile18, Ile22, Ala23, Ile24, Ala25, and Ile26). The residues from Ile18 to Ile26 formed a continuous hydrophobic surface.

3.5 Model structure of the CP1 and LPS complex

The CP1 structures in the LPS-bound state, which was calculated by the distance constraints obtained from Tr-NOE, were docked with LPS using AutoDock Vina software (Figure 7). I used the well-defined α-helical C-terminal region (Lys15–Gly29) of CP1 with LPS for docking calculations. LPS was assumed to be rigid and formed a 1:1 complex in the AutoDock calculation, consistent with the findings of other researchers [28,34,35]. In the majority of the complex structures, CP1 was oriented parallel to the long axis of the lipid A portion of LPS (Figure 7B). In those docking ensembles, the lowest binding free energy of docking in the LPS-bound state of CP1

was -4.4 kcal/mol, and the average binding free energy was -3.326 ± 0.323 kcal/mol. Lipid A consists of two glucosamine units with free phosphate groups that are linked to six acyl chains. The model structure of CP1 bound to LPS revealed the interaction between the side chains of two lysine residues (Lys15 and Lys16) and a diphosphate group of lipid A (Figure 7C). Five continuous residues (Ile22-Ala23-Ile24-Ala25-Ile26) were located near the acyl chain of LPS, and the side chains of Ile22 and Ile26 interacted with the acyl chain directly. Thus, two lysine residues likely interacted with the diphosphate group of lipid A by electrostatic interactions, and the hydrophobic surface was arranged according to the acyl chain of LPS by van der Waals interactions. Glu20 was located on the opposite surface, which interacts with the acyl chain of LPS; therefore, the negative charge of Glu20 may not interfere with the interaction between CP1 and LPS.

3.6 Determination of antimicrobial activity

The data from NMR and docking experiments suggested that the C-terminal region of CP1 may be critical for the interaction with LPS. Because LPS is the major component of the outer membrane of Gram-negative bacteria, the interaction between AMPs and LPS is thought to influence antimicrobial activity.

Therefore, I measured the MBCs of CP1 and CP1 analogs lacking the C-terminal amino acid residues using *E. coli* ML35 (Figure 8). The results showed that the MBC of CP1 was about 4 μM, whereas that of $CP1_{1-25}$ was 8 μM. In contrast, $CP1_{1-20}$, which lacked the putative LPS-binding region, had little antimicrobial activity against *E. coli* ML35. This result indicated that the α-helical C-terminal region contributed to the antimicrobial activity of CP1 against Gram-negative bacteria.

4. Discussion

Although CP1 is known to interact with LPS, no previous studies had reported the structure of CP1 bound to LPS [8]. In this study, I obtained structural information of isotopically labeled CP1 bound to LPS using Tr-NOE experiments. LPS-bound CP1 exhibited an α-helical structure at the C-terminal region (Lys15–Gly29). Interestingly, the well-structured region observed in this study was not consistent with that in previous studies using 30% 1,1,1,3,3,3-hexafluoro-2-propanol, in which CP1 exhibited a straight α-helical structure (Lys3-Gly29) over the entire molecule [16]. Additionally, the AutoDock calculation of the CP1/LPS complex showed that CP1 was aligned parallel to the plane of the long axis of LPS. The phosphate at the O1 position of GlcN II was found to interact with positively charged Lys15 and Lys16. Close packing was also observed between the hydrophobic residues Ile22 and Ile26 and the acyl chain of LPS. Thus, the docking results revealed that the C-terminal region of CP1 interacted with LPS via hydrophobic and electrostatic interactions, providing important insights into the interactions between these proteins and the potential antimicrobial mechanisms of AMPs.

Many studies have reported that positively charged amino acids play important roles in the initial interactions between AMPs and the phosphate in lipid A through creation of electrostatic interactions [11–13,26–28]. Interestingly, some peptides have similarities with CP1/lipid A binding in that two positively charged amino acids are contiguous to a phosphate group in lipid A. For example, RG16, which has half of an α-helical structure at the C-terminal region in LPS, has been shown to be have electrostatic interactions between two positively charged residues (Arg1 and Arg4) and the phosphate of GlcN II [28]. In the complex of YW12 with LPS, the residues Arg6

and Lys7 in the C-terminal β-turn are in close proximity to the phosphate group at GlcN I via ionic hydrogen bonds [36]. Similar to CP1, YW12 shows two sequential positively charged amino acids in close proximity with the negatively charged phosphate molecule.

The hydrophobic residues of the peptide are also able to interact with the lipid bilayer [37–40]. Some studies have revealed the importance of hydrophobic residues for antimicrobial activity [41,42]. I also confirmed that the antimicrobial activity of $CP1_{1\text{-}20}$, which has lower hydrophobicity, was decreased compared with the activity of CP1. The hydrophobic interaction can disrupt the arrangement of the lipid acyl chains and cause local disruption. In the LPS-bound structure of CP1, the α-helical structure aligned parallel to the polyacyl domain of LPS, and the hydrophobic residues Ile22 and Ile26 on the helix interact with the acyl chain of lipid A. In the case of RG16 with LPS, an α-helix fragment (Leu8–Ala15) was found to be aligned parallel to the acyl chain of LPS, similar to the LPS-bound state of CP1 [15]. In particular, there was close packing between Trp6, Leu8, Val9, Ile10, Val13, and Ile14 on the helix with the acyl chains of LPS. WR17 also has an α-helical structure at the N-terminal region in presence of LPS [43]. The structures of WR17 are stabilized by the hydrophobic packing of Trp1, Leu3, Leu4, and Ala7 with the acyl chain of LPS.

Several studies have also described the structures of other cecropin-type AMPs in the presence of LPS or mimetic membranes of Gram-negative bacteria. Table 2 shows a summary of the differences between cecropin-type AMPs in the LPS interaction. The LPS-bound state of Pa4, a cecropin-type AMP, adopts a unique helix-turn-helix conformation and resembles a “horseshoe” in LPS micelles [44]. In particular, Lys8 at the N-terminal helix and Lys16 at the C-terminal helix are expected to interact with the phosphate groups of GlcN I and GlcN II by salt-bridge or hydrogen bonding.

Some hydrophobic residues of each helix (e.g., Ile9, Ile10, Pro13, Leu18, Leu19, and Ala21) are located along the acyl chains of LPS. As a result, the structure is distinct from that of CP1, which had a straight C-terminal helix structure. In case of sarcotoxin IA, a 39-residue cecropin-type peptide, the peptide forms a helix-hinge-helix structure in methanol solution similar to other cecropin-type peptides [45]. On the other hand, in a DPC/lipid A mixture, the peptide exhibits an α-helix at its Leu3–Arg18 sequence within the N-terminal region, whereas the C-terminal region, which forms an α-helix in methanol, was unstructured [46]. These chemical shift changes between samples with or without the DPC/lipid A mixture indicated that the charged residues Lys4 and Lys5 were involved in the interaction with lipid A. The structures of sarcotoxin IA and CP1 bound to LPS are similar in that two sequential lysine residues on the helical structure participate in the interaction of the peptide and LPS, although the interacting regions are completely different. In the case of sarcotoxin IA, the highly conserved Trp2 in cecropin family proteins is thought to anchor into the hydrophobic environment and precede α-helix formation at the N-terminal region, whereas Trp2 of CP1 is not thought to participate in the interaction between the peptide and LPS. Interestingly, the 3D structures of CP1, Pa4, and sarcotoxin IA and the structures showing their interactions with LPS differ, despite that these three peptides are all part of the cecropin peptide family.

In summary, I constructed an overexpression system of CP1 to produce isotopically labeled CP1. Using ^{15}N-edited and ^{13}C-edited Tr-NOE experiments, I obtained structural information for LPS-bound CP1. The results showed that the C-terminal α-helical structure of CP1 played a crucial role in the recognition of LPS. I anticipate that these findings will be useful for studies of LPS recognition by AMPs.

This improved understanding of the molecular basis of AMP activity may assist in the future design of more specific and potent antibacterial agents.

5. Figures

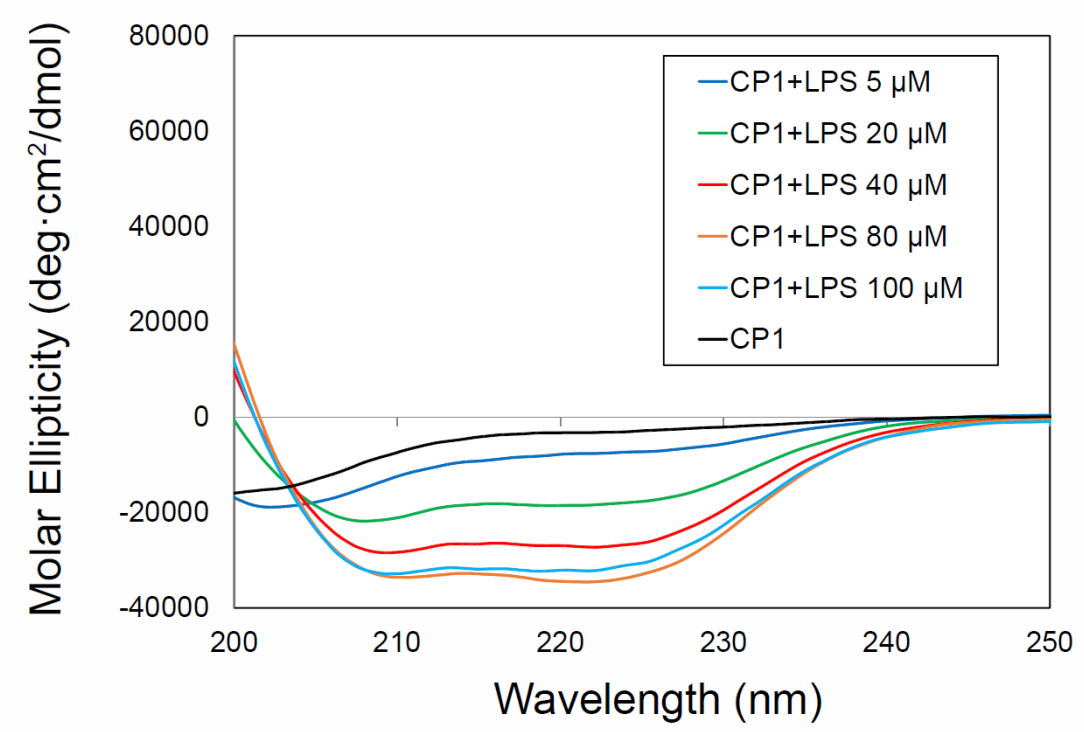

Figure 1. Secondary structures of 20 μM CP1 in free and LPS-bound forms, as determined by CD spectroscopy. CD spectra of CP1 were obtained at various concentrations of LPS (0, 5, 20, 40, 80, and 100 μM) from *E. coli* O111:B4 in 10 mM sodium phosphate (pH 6.0).

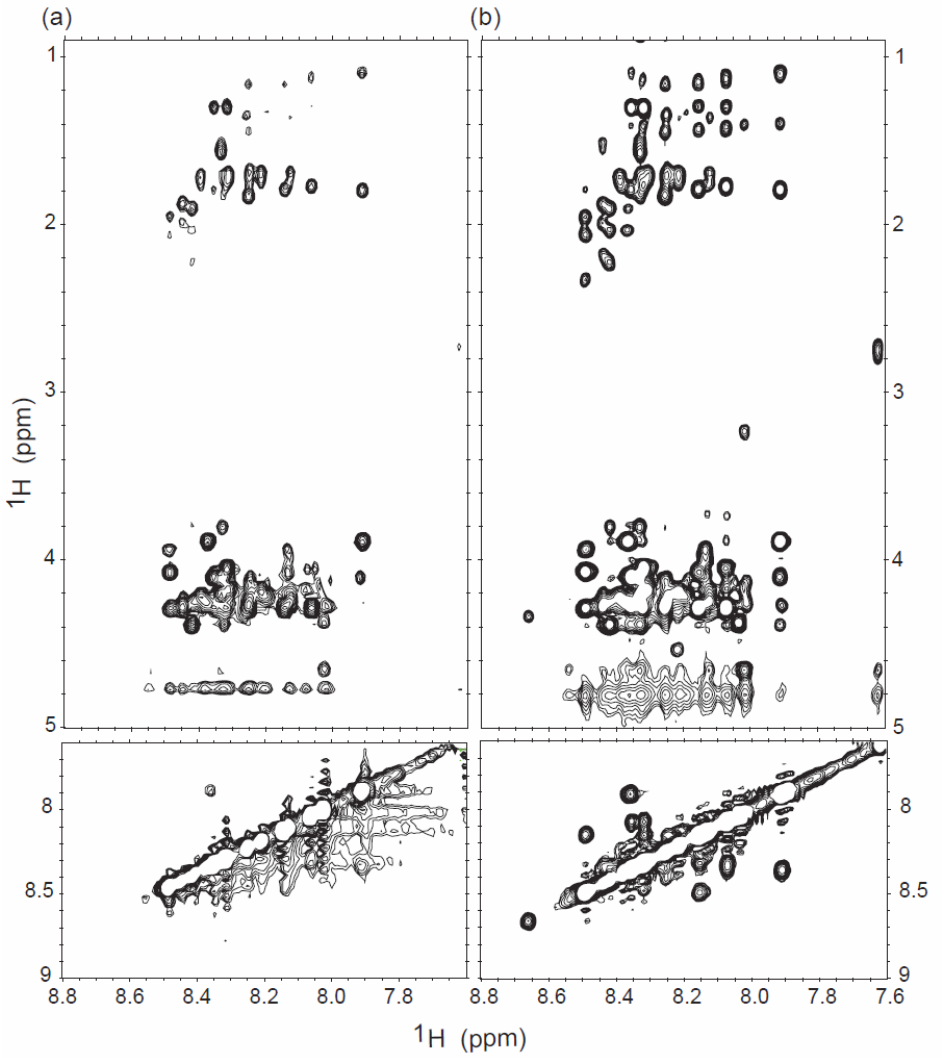

Figure 2. Two-dimensional NOESY spectra of CP1 with/without LPS. The fingerprint region and amide region of the NOESY spectra of CP1 showing HN-Hα, HN-HN, and HN side-chain resonances. (a) NOESY spectrum of CP1 in the absence of LPS and (b) the Tr-NOESY spectrum of CP1 in the presence of LPS showed a significant number of NOE cross-peaks compared with those in the free state. The Tr-NOESY spectra of CP1 were acquired in the presence of 50 μM LPS. Tr-NOESY experiments were carried out at 600 MHz and 298 K, with a mixing time of 150 ms.

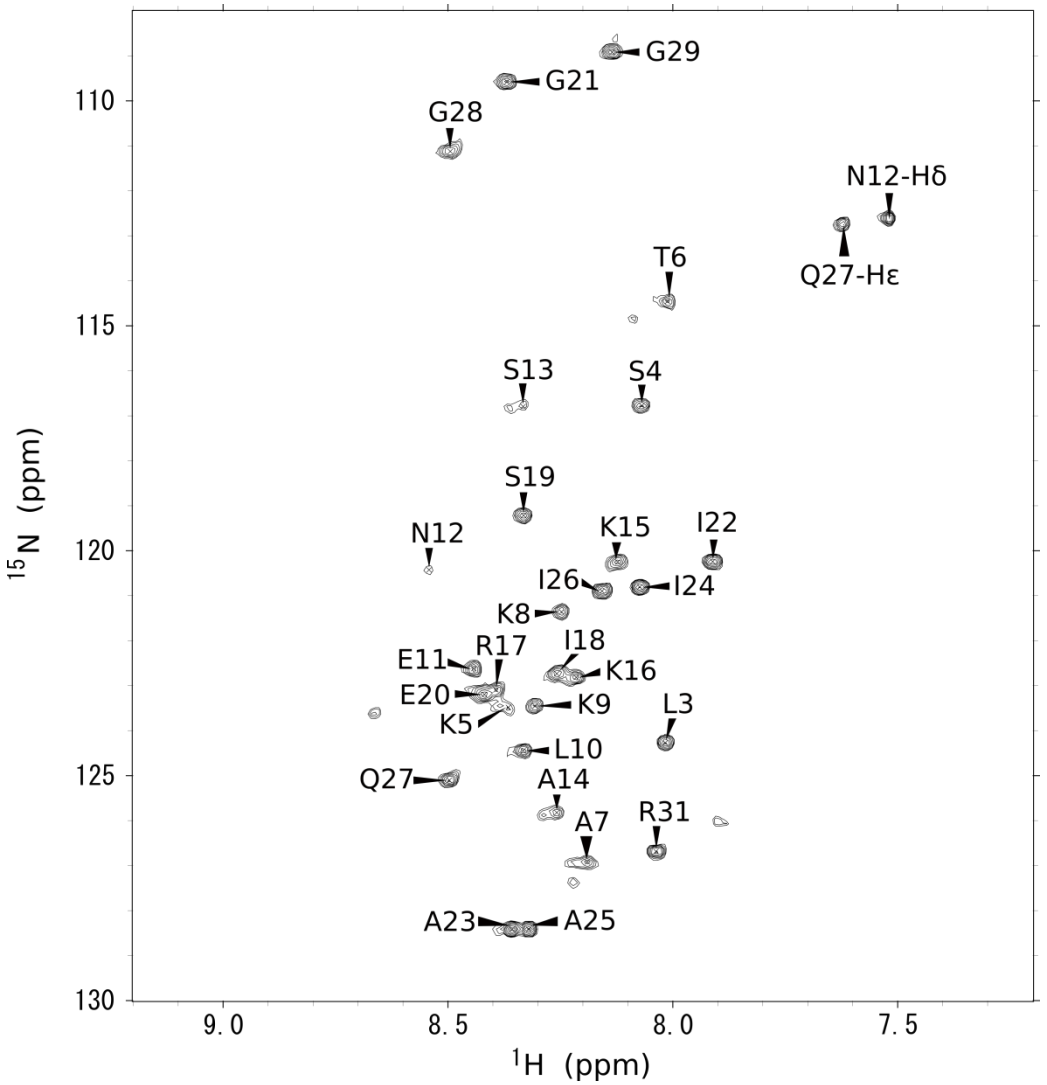

Figure 3. ^{1}H-^{15}N HSQC 600 MHz NMR spectrum of CP1 at pH 5.0 and 298 K. The spectrum showed excellent chemical shift dispersion, indicating a single species with no evidence of heterogeneity.

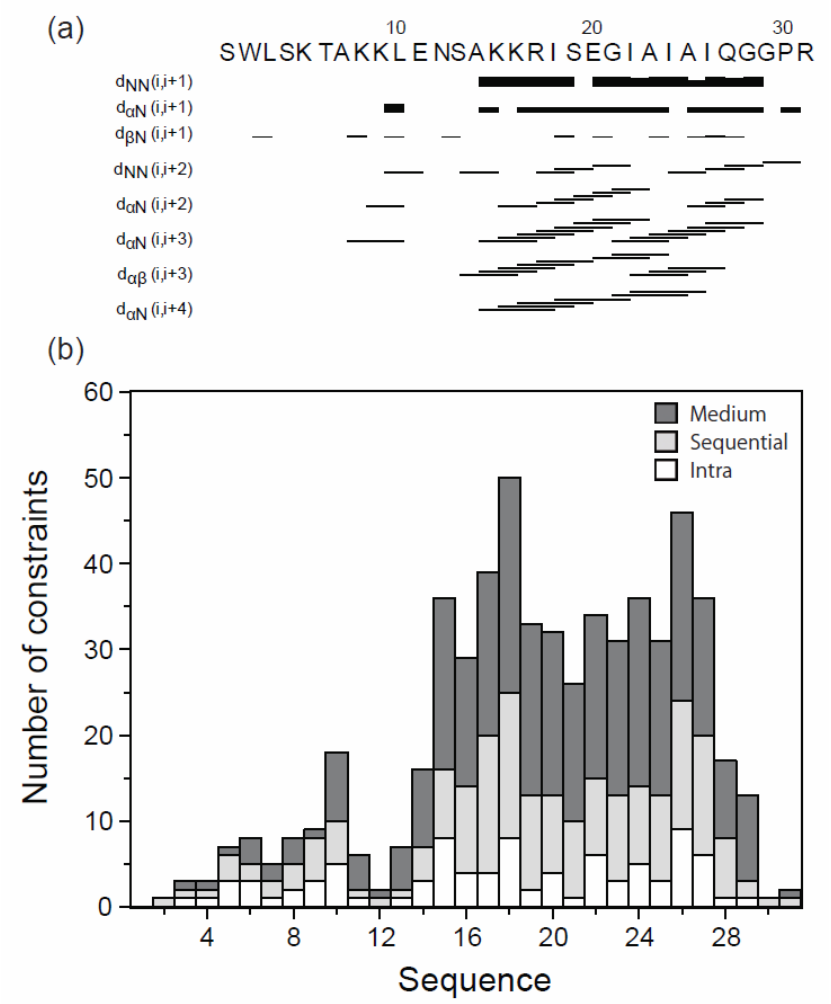

Figure 4. Summary of NMR structural parameters of CP1 in LPS micelles. (a) Bar diagram showing sequential and medium range NOEs of CP1 in the presence of LPS. The thickness of the bars indicates the intensity of the peaks, which are assigned as strong, medium, and weak. The amino acid sequence of CP1 is shown at the top. (b) A histogram showing the number of Tr-NOEs of CP1 as a function of residue number in complex with LPS micelles.

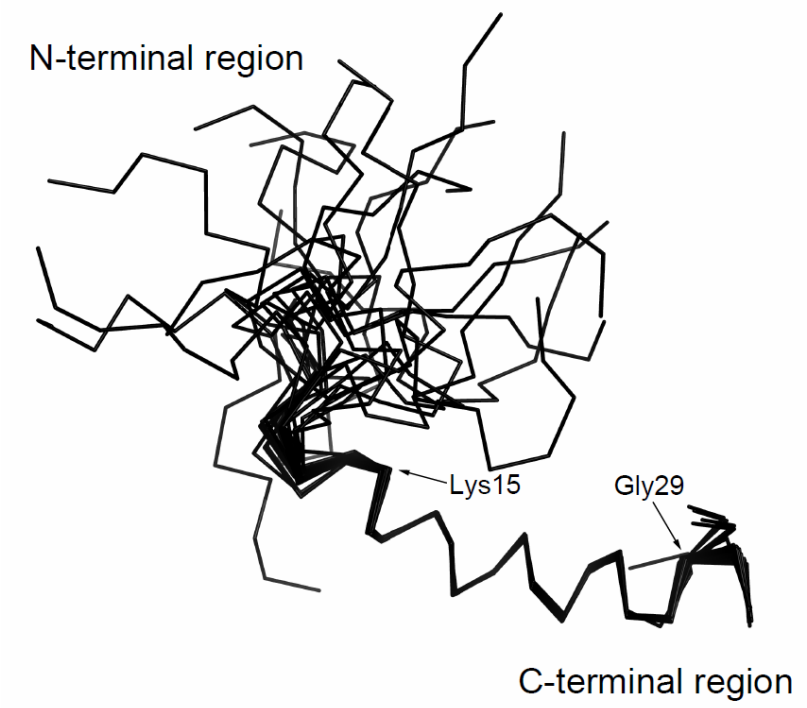

Figure 5. Backbone traces of the 20 lowest energy structures of CP1 bound to LPS, obtained from CYANA. CP1 in the LPS-bound state exhibits an α-helix structure along the residues from Lys15 to Gly29 in the C-terminal region.

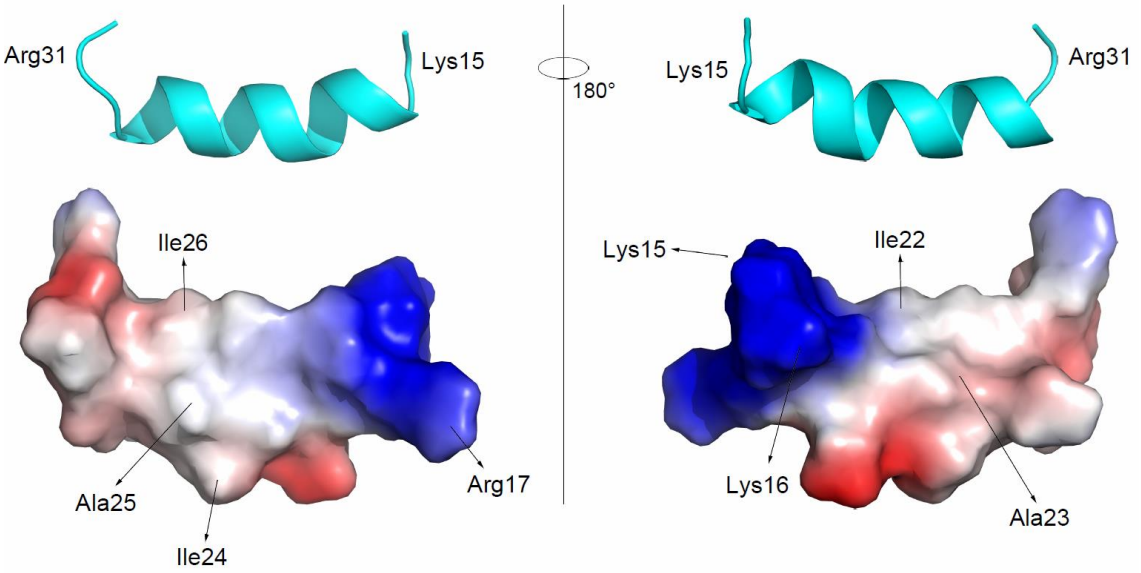

Figure 6. Representative ribbon conformations (upper) and electrostatic surface potentials (lower) of the LPS-bound CP1 (Lys15–Arg31) structure generated by PyMOL, where the positive potentials are drawn in blue, and the negative potentials are drawn in red.

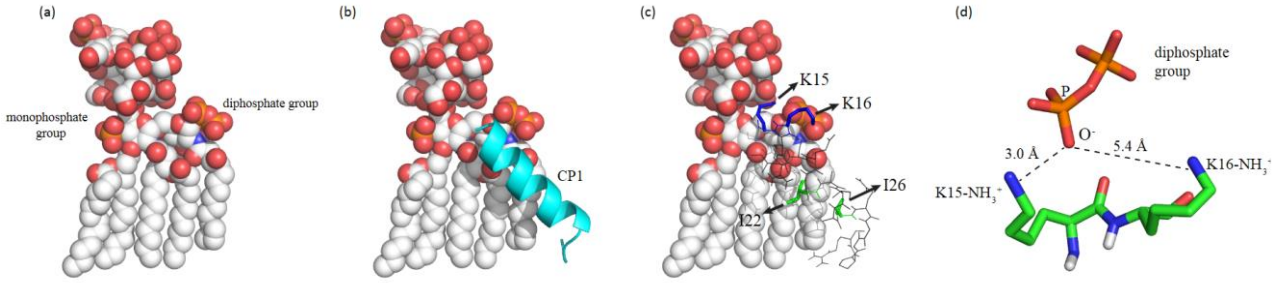

Figure 7. (a) LPS structure used in the docking calculation (PDB ID 1QFG). (b, c) The complex structure of CP1 and LPS. CP1 is shown as a cartoon (b) and sticks (c). (d) The distance between Lys15-NH3/Lys16-NH3 and phosphate group. The docking model was calculated by using the model structure of CP1 in its LPS-bound state and the crystal structure of LPS.

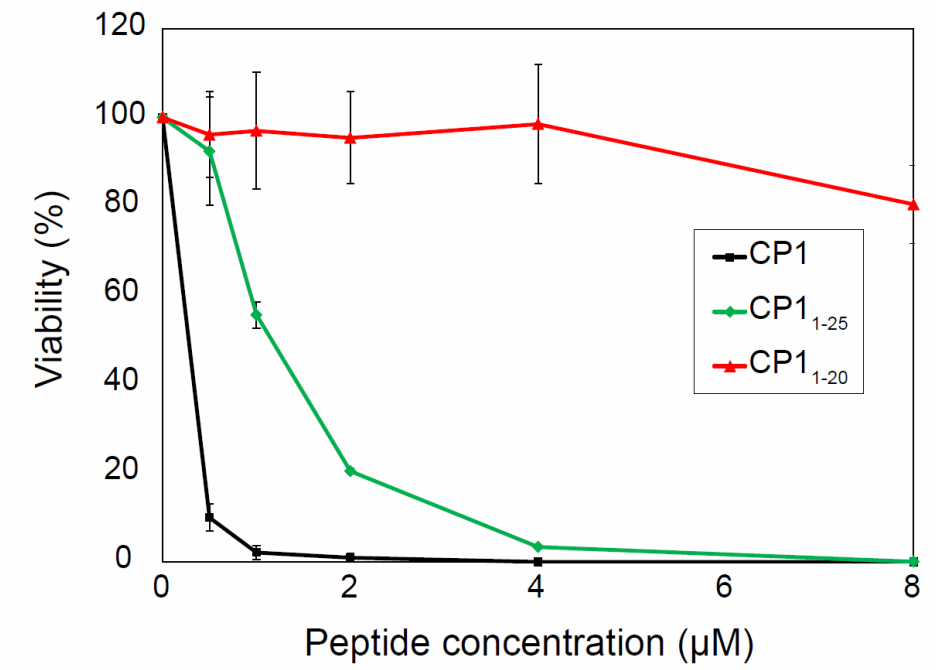

Figure 8. Viability of bacteria (*E. coli* ML35) exposed to different concentrations of CP1 and its analogs $CP1_{1-25}$ and $CP1_{1-20}$.

6. Tables

Table 1. Summary of the structural statistics for the 20 lowest energy structures of CP1 in its free and LPS-bound states.

Structural statistics of CP1 ensemble

Total no. of NOE restraints	
Intra-residue	98
Sequential	94
Medium-range	153
Long-range	1
total	337
Deviation from mean structure	
(only for the well-defined region K15-R31)	
Average backbone RMSD to mean (Å)	0.15 ± 0.07
Average heavy atom RMSD to mean (Å)	0.68 ± 0.10
Ramachandran plot analysis	
%Residues in the most favorable regions	68.0
%Residues in additionally allowed regions	21.8
%Residues in generously allowed regions	8.6
%Residues in disallowed regions	1.6

Table 2. The comparison of sequence, structure feature, and critical residues for interaction with LPS of cecropin-type antimicrobial peptides

Peptide [reference]	Sequence	Structure in LPS	Critical residues for interaction with LPS
Cecropin P1	SWLSKTAKKLENSAKKR ISEGIAIAIQGGPR	α-helix in C-terminal (K15-G29)	K15, K16, I22, I26
Sarcotoxin IA [44]	GWLKKIGKKIERVGQHT RDATIQGLGIAQQAANV AATAR	α-helix in N-terminal (L3-R18)	W2, K4, K5
Pa4 [46]	GFFALIPKIISSPLFKTLLS AVGSALSSSGGQE	helix(L5-S12)-turn-helix(K16-G31)	K8, K16, I9, I10, P13, L18, L19, A21

7. References

1. Brogden KA. Antimicrobial peptides: pore formers or metabolic inhibitors in bacteria? *Nat. Rev. Microbiol.* 2005; **3**: 238–250; DOI:10.1038/nrmicro1098.

2. Yeaman MR, Yount NY. Mechanisms of antimicrobial peptide action and resistance. *Pharmacol. Rev.* 2003; **55**: 27-55; DOI:10.1124/pr.55.1.2.

3. Lee JY, Boman A, Sun CX, Andersson M, Jörnvall H, Mutt V, Boman HG. Antibacterial peptides from pig intestine: isolation of a mammalian cecropin. *Proc. Natl. Acad. Sci. U. S. A.* 1989; **86**: 9159-9162.

4. Moore AJ, Beazley WD, Bibby MC, Devine DA. Antimicrobial activity of cecropins. *J. Antimicrob. Chemother.* 1996; **37**: 1077-1089; DOI:10.1093/jac/37.6.1077.

5. Giacometti A, Cirioni O, Barchiesi F, Fortuna M, Scalise G. In-vitro activity of cationic peptides alone and in combination with clinically used antimicrobial agents against *Pseudomonas aeruginosa*. *J. Antimicrob. Chemother.* 1999; **44**: 641-645.

6. Giacometti A, Cirioni O, Del Prete MS, Barchiesi F, Paggi AM, Petrelli E, Scalise G. Comparative activities of polycationic peptides and clinically used antimicrobial agents against multidrug-resistant nosocomial isolates of *Acinetobacter baumannii*. *J. Antimicrob. Chemother*. 2000; **46**: 807-810.

7. Wang Z, Han X, He N, Chen Z, Brooks CL. Molecular structures of C- and N-terminus cysteine modified cecropin P1 chemically immobilized onto maleimide-terminated self-assembled monolayers investigated by molecular dynamics simulation. *J. Phys. Chem. B* 2014; 118: 5670-5680; DOI:10.1021/jp5023482.

8. Strauss J, Kadilak A, Cronin C, Mello C, Camesano T. Binding, inactivation, and adhesion forces between antimicrobial peptide cecropin P1 and pathogenic *E. coli*. *Colloids Surf. B* 2009; **75**: 156-164; DOI:10.1016/j.colsurfb.2009.08.026.

9. Arcidiacono S, Pivarnik P, Mello CM, Senecal A. Cy5 labeled antimicrobial peptides for enhanced detection of *Escherichia coli* O157:H7. *Biosens. Bioelectron.* 2008; **23**: 1721-1727; DOI:10.1016/j.bios.2008.02.005.

10. Gazit E, Miller IR, Biggin PC, Sansom MS, Shai Y. Structure and orientation of the mammalian antibacterial peptide cecropin P1 within phospholipid membranes. *J. Mol. Biol.* 1996; **258**: 860-870; DOI:10.1006/jmbi.1996.0293.

11. Zhang L, Scott MG, Yan H, Mayer LD, Hancock RE. Interaction of polyphemusin I and structural analogs with bacterial membranes, lipopolysaccharide, and lipid monolayers. *Biochemistry* 2000; **39**: 14504-14514; DOI:10.1021/bi0011173.

12. Raetz CR, Whitfield C. Lipopolysaccharide endotoxins. *Ann. Rev. Biochem.* 2002; **71**: 635-700; DOI:10.1146/annurev.biochem.71.110601.135414.

13. Bhunia A, Saravanan R, Mohanram H, Mangoni ML, Bhattacharjya S. NMR structures and interactions of temporin-1Tl and temporin-1Tb with lipopolysaccharide micelles: mechanistic insights into outer membrane permeabilization and synergistic activity. *J. Biol. Chem.* 2011; **286**: 24394-24406; DOI:10.1074/jbc.M110.189662.

14. Japelj B, Pristovsek P, Majerle A, Jerala R. Structural origin of endotoxin neutralization and antimicrobial activity of a lactoferrin-based peptide. *J. Biol. Chem.* 2005; **280**: 16955-16961; DOI:10.1074/jbc.M500266200.

15. Avitabile C, Netti F, Orefice G, Palmieri M, Nocerino N, Malgieri G, D'Andrea LD, Capparelli R, Fattorusso R, Romanelli A. Design, structural and functional characterization of a temporin-1b analog active against Gram-negative bacteria. *Biochim. Biophys. Acta* 2013; **1830**: 3767-3775; DOI:10.1016/j.bbagen.2013.01.026.

16. Sipos D, Andersson M, Ehrenberg A. The structure of the mammalian antibacterial peptide cecropin P1 in solution, determined by proton-NMR. *Eur. J. Biochem.* 1992;

209: 163-169; DOI:10.1111/j.1432-1033.1992.tb17273.x.

17. Holak TA, Engström A, Kraulis PJ, Lindeberg G, Bennich H, Jones TA, Gronenborn AM, Clore GM. The solution conformation of the antibacterial peptide cecropin A: a nuclear magnetic resonance and dynamical simulated annealing study. *Biochemistry* 1988; **27**: 7620-7629.

18. Wu J-MM, Jan P-SS, Yu H-CC, Haung H-YY, Fang H-JJ, Chang Y-II, Cheng J-WW, Chen HM. Structure and function of a custom anticancer peptide, CB1a. *Peptides* 2009; **30**: 839-848; DOI:10.1016/j.peptides.2009.02.004.

19. Post CB. Exchange-transferred NOE spectroscopy and bound ligand structure determination. *Curr. Opin. Struct. Biol.* 2003; **13**: 581-588; DOI:10.1016/j.sbi.2003.09.012.

20. Xu X, Jin F, Yu X, Ji S, Wang J, Cheng H, Wang C, Zhang W. Expression and purification of a recombinant antibacterial peptide, cecropin, from *Escherichia coli*. *Protein Expr. Purif.* 2007; **53**: 293-301; DOI:10.1016/j.pep.2006.12.020.

21. Delaglio F, Grzesiek S, Vuister GW, Zhu G, Pfeifer J, Bax A. NMRPipe: a multidimensional spectral processing system based on UNIX Pipes. *J. Biomol. NMR* 1995; **6**: 277-293; DOI:10.1007/BF00197809.

22. Goddard TD, Kneller DG. SPARKY 3. *University of California, San Francisco*.

23. López-Méndez Blanca, Güntert Peter. Automated protein structure determination from NMR spectra. *J. Am. Chem. Soc.* 2006; **128**: 13112-13122; DOI:10.1021/ja061136l.

24. Laskowski RA, Rullmann JAC, MacArthur M, Kaptein R, Thornton JM. AQUA and PROCHECK-NMR: programs for checking the quality of protein structures solved by NMR. *J. Biomol. NMR* 1996; **8**: 477-486; DOI:10.1007/BF00228148.

25. The PyMOL Molecular Graphics System, Version 1.7.4 Schrödinger, LLC.

26. Trott O, Olson AJ. AutoDock Vina: improving the speed and accuracy of docking with a new scoring function, efficient optimization, and multithreading. *J. Comput. Chem.* 2010; **31**: 455-461; DOI:10.1002/jcc.21334.

27. Ferguson AD, Welte W, Hofmann E, Lindner B, Holst O, Coulton JW, Diederichs K. A conserved structural motif for lipopolysaccharide recognition by procaryotic and eucaryotic proteins. *Structure* 2000; **8**: 585-592; DOI:10.1016/S0969-2126(00)00143-X.

28. Bhunia A, Mohanram H, Bhattacharjya S. Lipopolysaccharide bound structures of the active fragments of fowlicidin-1, a cathelicidin family of antimicrobial and antiendotoxic peptide from chicken, determined by transferred nuclear Overhauser effect spectroscopy. *Biopolymers* 2009; **92**: 9-22; DOI:10.1002/bip.21104.

29. G Greenfield NJ. Using circular dichroism spectra to estimate protein secondary structure. *Nat. Protoc.* 2006; **1**: 2876-2890; DOI:10.1038/nprot.2006.202.

30. Louis-Jeune C, Andrade-Navarro MA, Perez-Iratxeta C. Prediction of Protein Secondary Structure from Circular Dichroism Using Theoretically Derived Spectra. *Proteins* 2012; **80**: 374–381; DOI:10.1002/prot.23188.

31. Yu L, Tan M, Ho B, Ding JL, Wohland T. Determination of Critical Micelle Concentrations and Aggregation Numbers by Fluorescence Correlation Spectroscopy: Aggregation of a Lipopolysaccharide. Anal. Chim. Acta 2006; 556: 216–225; DOI:10.1016/j.aca.2005.09.008.

32. Wang Z, Jones JD, Rizo J, Gierasch LM. Membrane-bound conformation of a signal peptide: a transferred nuclear Overhauser effect analysis. *Biochemistry* 1993; **32**: 13991-13999; DOI:10.1021/bi00213a032.

33. Lee MS, Cao B. Nuclear Magnetic Resonance Chemical Shift: Comparison of

Estimated Secondary Structures in Peptides by Nuclear Magnetic Resonance and Circular Dichroism. *Protein Eng.* 1996; **9**: 15–25.

34. Bhunia A, Chua GL, Domadia PN, Warshakoon H, Cromer JR, David SA, Bhattacharjya S. Interactions of a Designed Peptide with Lipopolysaccharide: Bound Conformation and Anti-Endotoxic Activity. *Biochem. Biophys. Res. Commun.* 2008; **369**: 853–857; DOI:10.1016/j.bbrc.2008.02.105.

35. Kushibiki T, Kamiya M, Aizawa T, Kumaki Y, Kikukawa T, Mizuguchi M, Demura M, Kawabata S, Kawano K. Interaction between Tachyplesin I, an Antimicrobial Peptide Derived from Horseshoe Crab, and Lipopolysaccharide. *Biochim. Biophys. Acta* 2014; **1844**: 527–534; DOI:10.1016/j.bbapap.2013.12.017.

36. Bhattacharjya S, Domadia PN, Bhunia A, Malladi S, David SA. High-resolution solution structure of a designed peptide bound to lipopolysaccharide: transferred nuclear Overhauser effects, micelle selectivity, and anti-endotoxic activity. *Biochemistry* 2007; **46**: 5864-5874; DOI:10.1021/bi6025159.

37. Stark M, Liu L-PP, Deber CM. Cationic hydrophobic peptides with antimicrobial activity. *Antimicrob. Agents Chemother.* 2002; **46**: 3585-3590; DOI:10.1128/AAC.46.11.3585-3590.2002.

38. Dathe M, Schümann M, Wieprecht T, Winkler A, Beyermann M, Krause E, Matsuzaki K, Murase O, Bienert M. Peptide helicity and membrane surface charge modulate the balance of electrostatic and hydrophobic interactions with lipid bilayers and biological membranes. *Biochemistry* 1996; **35**: 12612-12622; DOI:10.1021/bi960835f.

39. Kim J-K, Lee E, Shin S, Jeong K, Lee J-Y, Bae S-Y, Kim S-H, Lee J, Kim S-R, Lee D-G, Hwang J-S, Kim Y. Structure and function of papiliocin with antimicrobial and

anti-inflammatory activities isolated from the swallowtail butterfly, *Papilio xuthus*. *J. Biol. Chem.* 2011; **286**: 41296-41311; DOI:10.1074/jbc.M111.269225.

40. Pristovsek P, Kidric J. Solution structure of polymyxins B and E and effect of binding to lipopolysaccharide: an NMR and molecular modeling study. *J. Med. Chem.* 1999; **42**: 4604-4613; DOI:10.1021/jm991031b.

41. Strandberg E, Zerweck J, Horn D, Pritz G, Berditsch M, Bürck J, Wadhwani P, Ulrich AS. Influence of hydrophobic residues on the activity of the antimicrobial Peptide Magainin 2 and Its Synergy with PGLa. *J. Pept. Sci.* 2015; **21**: 436–445; DOI:10.1002/psc.2780.

42. Chen Y, Guarnieri MT, Vasil AI, Vasil ML, Mant CT, Hodges RS. Role of peptide hydrophobicity in the mechanism of action of alpha-helical antimicrobial peptides. *Antimicrob. Agents Chemother.* 2007; **51**: 1398–1406; DOI:10.1128/AAC.00925-06.

43. Ghosh A, Datta A, Jana J, Kar RK, Chatterjee C, Chatterjee S, Bhunia A. Sequence context induced antimicrobial activity: insight into lipopolysaccharide permeabilization. *Mol. BioSyst.* 2014; **10**: 1596-1612; DOI:10.1039/c4mb00111g.

44. Bhunia A, Domadia PN, Torres J, Hallock KJ, Ramamoorthy A, Bhattacharjya S. NMR structure of pardaxin, a pore-forming antimicrobial peptide, in lipopolysaccharide micelles: mechanism of outer membrane permeabilization. *J. Biol. Chem.* 2010; **285**: 3883-3895; DOI:10.1074/jbc.M109.065672.

45. Iwai H, Nakajima Y, Natori S, Arata Y, Shimada I. Solution conformation of an antibacterial peptide, sarcotoxin IA, as determined by 1H-NMR. *Eur. J. Biochem.*1993; **217**: 639-644; DOI:10.1111/j.1432-1033.1993.tb18287.x.

46. Yagi-Utsumi M, Yamaguchi Y, Boonsri P, Iguchi T, Okemoto K, Natori S, Kato K. Stable isotope-assisted NMR characterization of interaction between lipid A and

sarcotoxin IA, a cecropin-type antibacterial peptide. *Biochem. Biophys. Res. Commun.* 2013; **431**: 136-140; DOI:10.1016/j.bbrc.2013.01.009.

8. Supporting Information

Table S1. Chemical Shift Assignments for cecropin P1 (CP1) in LPS.

Residue	HN	N	CA	HA	CB	HB	Other
W2		129.548	57.773	4.708	29.428	3.288	HE 10.12, 7.32 HZ 6.86 HZ 7.28 HH 6.97
L3	8.017	124.271	55.161	4.217	42.595	1.454	CG 26.705 CD 24.72, 23.598 HD 0.769, 0.837
S4	8.069	116.777	58.722	4.384	63.644	3.795	
K5	8.366	123.484	56.433	4.265	32.944	1.786, 1.747	CG 24.752 CD 29.053 CE 42.111 HG 1.4, 1.451 HD 1.666 HE 2.979
T6	8.012	114.457	61.932	4.271	69.714	4.175	CG 21.579
A7	8.19	126.921	52.428	4.344	19.24	1.382	
K8	8.248	121.357	56.433	4.265	32.935	1.789, 1.747	CG 24.756 CD 29.02 CE 42.103 HG 1.4, 1.451 HD 1.666 HE 2.978
K9	8.306	123.451	56.433	4.265	32.948	1.785, 1.749	CG 24.748 CD 29.061 CE 42.103 HG 1.399, 1.449 HD 1.666 HE 2.978
L10	8.333	124.445	55.111	4.344	42.224	1.632, 1.563	CG 27.262 CD 24.829, 23.512 HG 1.471 HD 0.866, 0.919
E11	8.443	122.625	58.417	4.286	30.397	2.067, 1.945	CG 36.121 HG 2.245
N12	8.542	120.43	53.552	4.77	38.839	2.834, 2.789	
S13	8.333	116.797	58.447	4.438	63.701	3.891	
A14	8.258	125.821	52.728	4.297	18.923	1.401	
K15	8.123	120.251	56.433	4.265	32.935	1.785, 1.746	CG 24.736 CD 29.061 CE 42.136 HG 1.399, 1.449 HD 1.667 HE 2.978
K16	8.215	122.812	56.433	4.265	32.944	1.788, 1.745	CG 24.736 CD 29.053 CE 42.111 HG 1.4, 1.451 HD 1.666 HE 2.979
R17	8.393	123.095	56.807	4.315	30.788	1.828, 1.763	CG 27.032 CD 43.403 HG 1.616 HD 3.194

I18	8.256	122.717	61.379	4.169	38.81	1.842	CG 27.242, 17.413 CD 12.856 HG 1.183, 1.183 HD 0.854
S19	8.332	119.218	58.458	4.443	63.668	3.861	
E20	8.419	123.197	58.417	4.286	30.43	2.034, 1.925	CG 36.295 HG 2.275
G21	8.369	109.576	45.334	3.942			
I22	7.911	120.245	61.113	4.159	38.81	1.842	CG 27.242, 17.413 CD 12.856 HG 1.183, 1.183 HD 0.854
A23	8.357	128.416	52.428	4.344	19.106	1.354	
I24	8.073	120.81	61.072	4.123	38.81	1.842	CG 27.242, 17.413 CD 12.856 HG 1.183, 1.183 HD 0.854
A25	8.32	128.412	52.428	4.344	19.09	1.352	
I26	8.157	120.896	61.072	4.123	38.81	1.842	CG 27.242, 17.413 CD 12.856 HG 1.183, 1.183 HD 0.854
Q27	8.497	125.104	56.112	4.342	29.333	2.107, 2.016	CG 33.68 HG 2.381
G28	8.495	111.121	45.176	3.992			
G29	8.135	108.917	44.477	4.056, 4.156			
P30			63.425	4.427	32.031	1.966, 2.271	CG 27.132 CD 49.792 HG 2.017 HD 3.619
R31	8.037	126.687	57.374	4.185	31.57	1.86, 1.714	CG 27.093 CD 43.401 HG 1.652 HD 3.195

Acknowledgements

I would like to express my deepest gratitude to by Professor Keiichi Kawano and Associate Professor Tomoyasu Aizawa for their patient guidance and assistance for my research and life in Japan. I am also thankful to Professor Makoto Demura, Associate Professor Takashi Kikukawa, Assistant Professor Masakatsu Kamiya and Dr. Yasuhiro Kumaki for their support and advice.

I am also appreciative of Professor Min Yao in reviewing this article.

Finally thank my family and friends for their faith in me and encouragement during my campus life in Hokkaido University.